

Investigation on microstructures and properties of semi-solid $\text{Al}_{80}\text{Mg}_5\text{Li}_5\text{Zn}_5\text{Cu}_5$ light-weight high-entropy alloy during isothermal heat treatment process

*Yong Hu^{1,2}, Yuan-yuan Liu^{1,2}, Long-zhi Zhao^{1,2}, Yan-chuan Tang^{1,2}, Hai-tao Jiao^{1,2}, and De-jia Liu^{1,2}

1. State Key Laboratory of Performance Monitoring Protecting of Rail Transit Infrastructure, East China Jiaotong University, Nanchang 330013, China

2. School of Materials Science and Engineering, East China Jiaotong University, Nanchang 330013, China

Abstract: The $\text{Al}_{80}\text{Mg}_5\text{Li}_5\text{Zn}_5\text{Cu}_5$ light-weight high-entropy alloy with globular microstructure was fabricated by isothermal heat treatment. The effects of isothermal temperatures and holding times on the semi-solid microstructure evolution were investigated. The results indicate that, with increase of the isothermal temperature, the average grain size increases and the spheroidization time shortens. With prolongation of holding time, the shape factor increases firstly and then decreases, and the average grain size decreases at first and then increases when the isothermal temperature is below 520 °C, however it increases gradually at 540 °C. The optimal semi-solid microstructure is obtained at 520 °C for 30 min, whose shape factor and average grain size are 0.90 and 56.4 μm, respectively. Compared with as-cast $\text{Al}_{80}\text{Mg}_5\text{Li}_5\text{Zn}_5\text{Cu}_5$ light-weight high-entropy alloy, the compressive strength and plasticity of semi-solid $\text{Al}_{80}\text{Mg}_5\text{Li}_5\text{Zn}_5\text{Cu}_5$ light-weight high-entropy alloy are increased by 36% and 108%, respectively. The formation of semi-solid microstructures includes three stages: melting separation, spheroidization, and coarsening growth. The sluggish diffusion effect of $\text{Al}_{80}\text{Mg}_5\text{Li}_5\text{Zn}_5\text{Cu}_5$ light-weight high-entropy alloy leads to a low coarsening rate, resulting in slow grain growth.

Keywords: light-weight high-entropy alloy; semi-solid; isothermal heat treatment; microstructure

CLC numbers: TG146.21; Document code: A; Article ID: 1672-6421(2022)06-519-09



*Yong Hu

Male, born in 1982, Ph. D., Professor. His research interests mainly focus on light-weight metal materials and the semi-solid process. To date, he has published about 60 papers.

E-mail: huyong@ecjtu.edu.cn

Received: 2022-05-26

Accepted: 2022-08-23

1 Introduction

High-entropy alloys have a wide application prospect as structural and functional materials due to their superior properties such as high strength and hardness, strong oxidation resistance, outstanding wear and corrosion resistance [1-4]. Generally, high-entropy alloys are composed of high-density transition metal elements such as Co, Cr, Fe, etc., which are difficult to meet the demands for light-weight and high-speed in the field of rail transportation [5, 6]. To broaden the application of high-entropy alloys, many researchers have dedicated themselves to the further development of light-weight high-entropy alloys. Du et al. [7] prepared MgCaAlLiCu high-entropy alloy with the density of 2.2 g·cm⁻³ by vacuum melting, which exhibited the compressive strength of 910 MPa. Stepanov et al. [8] reported an AlNbTiVZr_{0.5} high-entropy alloy fabricated by arc melting with a density of 5.64 g·cm⁻³ and a compressive strength of 1,485 MPa. The specific strength of the alloy at high temperature is higher than that of Ni and Ti alloys. However, the main obstacle for further using such materials is the difficulty in forming due to their low plasticity caused by defects such as coarse dendritic structure, uneven composition and high porosity of casting high-entropy alloys [9, 10].

Semi-solid metal forming has the advantages of good fluidity and low deformation resistance because it combines the characteristics of liquid forming and plastic forming [11],

and provides the possibility for forming the low-plasticity high-entropy alloys. The most crucial step of the semi-solid metal forming process is to obtain the fine, uniform non-dendritic globular microstructure. At present, the required globular microstructure can be obtained by either a liquid route^[12] or a solid route^[13]. Compared to the former, the solid route delivers a relatively compact billet with the benefit of no contamination and wide application possibilities.

The solid route mainly includes the strain induced melt activated method (SIMA)^[14], recrystallization and partial melting method (RAP)^[15] and isothermal heat treatment method^[16]. In recent years, RAP has been the primary method applied to acquire the globular microstructure of high-entropy alloys. Zhang et al.^[17] demonstrated that, compared with the conventional alloy such as aluminium alloys and magnesium alloys, CoCrCuFeNi high-entropy alloy had a low coarsening rate in semi-solid state, which was commonly attributed to the sluggish diffusion effect of high-entropy alloy. Wang et al.^[18] pointed out that the plasticity of semi-solid CoCrCuFeNi high-entropy alloy was enhanced from 10.2% to 13.7% comparing to the rolled CoCrCuFeNi high-entropy alloy. Nevertheless, RAP needs to carry out large plastic deformation of the alloy prior to reheating, which has a complex process, high energy consumption and low efficiency. The isothermal heat treatment method omits the special procedure of plastic deformation to fabricate the semi-solid materials, but obtains the non-dendritic globular microstructure during the heating process prior to semi-solid thixoforming. Thus, there is great potential in semi-solid metal processing.

The aim of this work is to investigate the effect of holding temperature and holding time on the microstructural evolution of the semi-solid Al₈₀Mg₅Li₅Zn₅Cu₅ light-weight high-entropy alloy during the isothermal heat treatment process. Moreover, the spheroidal mechanism and coarsening kinetics of semi-solid microstructure are discussed in detail.

2 Experimental materials and methods

Al₈₀Mg₅Li₅Zn₅Cu₅ high-entropy alloy was produced using ingredients of Al, Mg, Li, Zn and Cu of 99.9% purity in a magnetic suspension furnace. The melt was cast into a copper mold with the size of $\Phi 50$ mm \times 300 mm.

The differential thermal analysis (DTA) curve of Al₈₀Mg₅Li₅Zn₅Cu₅ high-entropy alloy was measured using NETZSCH STA449 F3 at the heating rate of 10 °C·min⁻¹. The DTA curve is shown in Fig. 1(a), which shows the solidus temperature and liquidus temperature are 480 °C and 580 °C, respectively. The solidus - liquidus temperature range is about 100 °C, which is suitable for semi-solid metal forming.

The samples with a dimension of $\Phi 10$ mm \times 10 mm were heated in a box-type resistance furnace with temperature fluctuation range of 1 °C, followed by water quenching at room temperature. The liquid volume fraction or solid volume fraction has great influence on the semi-solid metal forming. Generally, the Scheil function can be used to calculate the liquid volume fraction or solid volume fraction. However, it is difficult to obtain the value of the partition coefficient *k* for high-entropy alloys. Kim et al.^[19] argued that the liquid volume fraction can be determined at different temperatures by the area ratio under the exothermic region. The liquid volume fraction can be expressed as: $f_l = A/A_{tot} = \int_{T_s}^T \Delta P dt / \int_{T_s}^{T_L} \Delta P dt$, where *A* is the integrated area of the heat absorption peak at different temperatures, *A*_{tot} is the total integrated area of the heat absorption peak, ΔP is the heat flow value, and *T*_s and *T*_L are solidus temperature and liquidus temperature, respectively. The liquid volume fraction (*f*_l) can be obtained by integrating the DTA curve in small steps, as is shown in Fig. 1(b). According to Fig. 1, the isothermal temperatures were selected as 500 °C (*f*_l=15%), 520 °C (*f*_l=42%) and 540 °C (*f*_l=58%), and the holding times were selected as 5 min, 15 min, 30 min, and 60 min, respectively.

The metallographic samples were etched using Keller reagent (1 mL HF+2.5 mL HNO₃+1.5 mL HCl+95 mL H₂O). The microstructures were observed using Axio vert.A1 optical microscopy (OM), Hitachi SU-8020 scanning electron microscopy (SEM) and UK-Oxford electron-back scattered diffraction (EBSD). The chemical compositions of different phases were analyzed by energy dispersive spectroscopy (EDS). The X-ray diffraction (XRD) measurements of the phase constitutions were performed using XRD-6100 diffractometer (Cu K α radiation with 40.0 kV anodic voltage, 30.0 mA current, 10°-90° scanning angle, and 2°·min⁻¹ scanning speed). Compression properties were tested on an electronic universal testing machine.

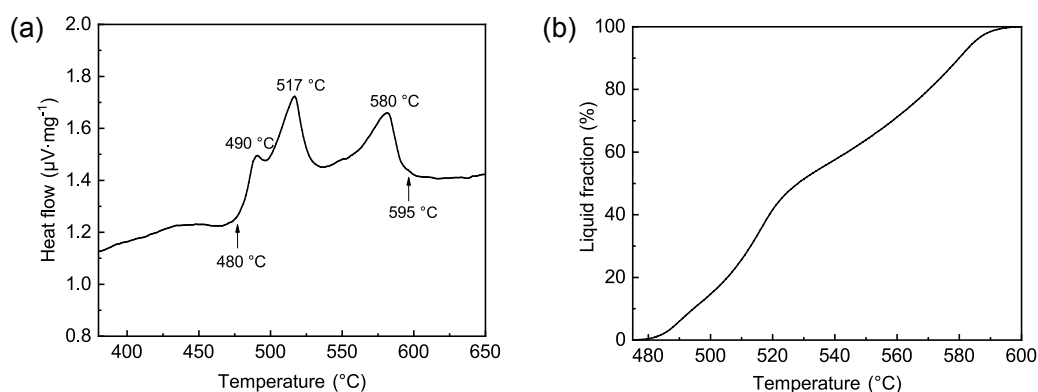


Fig. 1: DTA curve (a) and liquid volume fraction (b) of Al₈₀Mg₅Li₅Zn₅Cu₅ light-weight high-entropy alloy

The average grain size and shape factor were analyzed using Image Pro-Plus software and calculated as follows^[20, 21]:

$$D = \frac{1}{N} \sum_{i=1}^N \sqrt{\frac{4A_i}{\pi}} \quad (1)$$

$$F = \frac{1}{N} \sum_{i=1}^N \frac{4\pi A_i}{P_i^2} \quad (2)$$

where D is the average grain size, μm ; A_i is the area of the i th grain, μm^2 ; F is the shape factor; P_i is the perimeter of the i th grain, μm ; N is the total number of grains. Where $0 \leq F \leq 1$, the closer the value is to 1, the better the spherification of the grain.

3 Results

3.1 Density

The theoretical density of $\text{Al}_{80}\text{Mg}_5\text{Li}_5\text{Zn}_5\text{Cu}_5$ high-entropy alloy can be estimated using a rule of mixtures assumption based on a disordered solid solution, as given by^[22]:

$$\rho = \frac{\sum_{i=1}^n C_i A_i}{\sum_{i=1}^n C_i A_i / \rho_i} \quad (3)$$

where A_i , ρ_i , C_i are the atomic weight, density and atomic percentage of the i th principal element, respectively. The standard atomic weight (A) and density (ρ) of elements can be seen in Table 1. According to the data of Table 1 and Eq. (3), the density of $\text{Al}_{80}\text{Mg}_5\text{Li}_5\text{Zn}_5\text{Cu}_5$ high-entropy alloy was calculated to be $2.87 \text{ g}\cdot\text{cm}^{-3}$.

The actual density (ρ') of $\text{Al}_{80}\text{Mg}_5\text{Li}_5\text{Zn}_5\text{Cu}_5$ high-entropy alloy can be calculated as follows:

$$\rho' = m_1 \times \rho_1 / (m_1 - m_2) \quad (4)$$

where ρ_1 is the density of the analytically pure alcohol ($0.790 \text{ g}\cdot\text{mL}^{-1}$), m_1 is the weight of the samples measured in the air, and m_2 is the weight of the samples measured in the analytically pure alcohol. According to Eq. (4), the actual density of $\text{Al}_{80}\text{Mg}_5\text{Li}_5\text{Zn}_5\text{Cu}_5$ high-entropy alloy was calculated to be $2.89 \text{ g}\cdot\text{cm}^{-3}$, which is close

Table 1: Standard atomic weight (A) and density (ρ) of elements

Element	A ($\text{g}\cdot\text{mol}^{-1}$)	ρ ($\text{g}\cdot\text{cm}^{-3}$)
Al	26.98	2.70
Mg	24.31	1.74
Li	6.94	0.54
Zn	65.41	7.13
Cu	63.55	8.93

to the theoretical calculation value. As defined by Gupta et al.^[23] for high-entropy alloys, when the density of high-entropy alloy is less than $3 \text{ g}\cdot\text{cm}^{-3}$, it is a light-weight high-entropy alloy. Therefore, $\text{Al}_{80}\text{Mg}_5\text{Li}_5\text{Zn}_5\text{Cu}_5$ fits the definition of a light-weight high-entropy alloy.

3.2 As-cast microstructure

Figure 2 shows the as-cast microstructure and XRD pattern of $\text{Al}_{80}\text{Mg}_5\text{Li}_5\text{Zn}_5\text{Cu}_5$ light-weight high-entropy alloy. It can be seen from Fig. 2(a) that the as-cast $\text{Al}_{80}\text{Mg}_5\text{Li}_5\text{Zn}_5\text{Cu}_5$ light-weight high-entropy alloy is mainly composed of a white dendritic and discontinuous mesh-like microstructure. As shown in Fig. 2(b), the alloy is composed of Al, Al_2Cu , MgZn_2 , Li_3CuAl_5 , and some unknown phases, which will be further investigated in our following work. The XRD pattern indicates that solid solution and intermetallic compounds are formed in $\text{Al}_{80}\text{Mg}_5\text{Li}_5\text{Zn}_5\text{Cu}_5$ light-weight high-entropy alloy. The results are in accordance with other light-weight high-entropy alloys obtained by Shao et al^[24].

3.3 Semi-solid microstructure

The semi-solid microstructures of $\text{Al}_{80}\text{Mg}_5\text{Li}_5\text{Zn}_5\text{Cu}_5$ light-weight high-entropy alloy held at different isothermal temperatures ($500 \text{ }^\circ\text{C}$, $520 \text{ }^\circ\text{C}$ and $540 \text{ }^\circ\text{C}$) for different holding times (5 min, 15 min, 30 min and 60 min) are shown in Fig. 3. As shown in Fig. 3(a), the microstructure shows still dendrites when holding at $500 \text{ }^\circ\text{C}$ for 5 min, but finer than that of the as-cast samples. When holding at $500 \text{ }^\circ\text{C}$ for 15 min, as shown

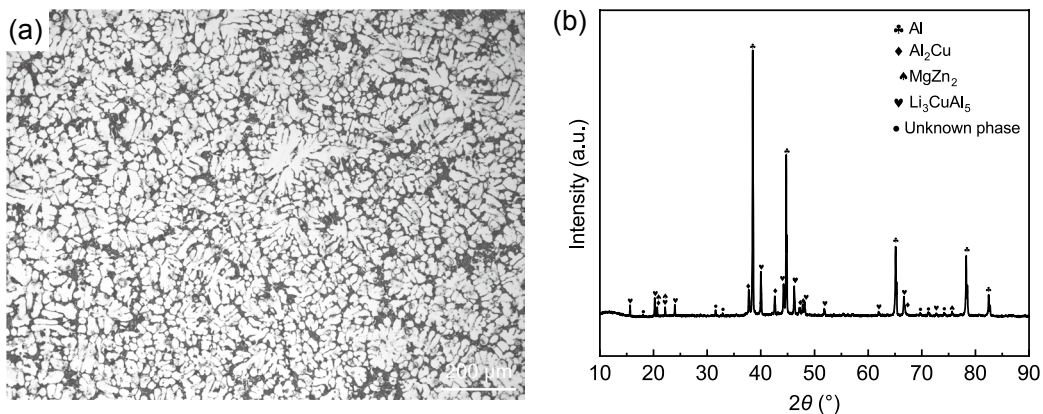


Fig. 2: Microstructure (a) and XRD pattern (b) of as-cast $\text{Al}_{80}\text{Mg}_5\text{Li}_5\text{Zn}_5\text{Cu}_5$ light-weight high-entropy alloy

in Fig. 3(b), the dendritic arms are fused and the grains become irregular polygonal shape with uneven size, which are separated by the liquid phase. When holding at 500 °C for 30 min, the liquid volume fraction is increased, and the globular grains are distributed uniformly in the liquid phase, as shown in Fig. 3(c). On further increasing the holding time to 60 min, the inhomogeneity of grains size is increased and the sphericity of the grains is decreased, as shown in Fig. 3(d). A similar phenomenon can be observed when the holding temperatures are 520 °C and 540 °C, respectively.

It can also be seen from Fig. 3 that, with increasing the isothermal temperature, the spheroidization time of the grains shortens and the grain size increases. When the isothermal temperature is 520 °C, compared with 500 °C, the dendritic grains basically disappear after holding for 5 min, as shown in Fig. 3(e). The globular and uniformly distributed grains appear at 30 min, as shown in Fig. 3(g). When the isothermal temperature is 540 °C, the globular grains can be clearly observed at 15 min [Fig. 3(j)], while the grains have merged to grow up at 30 min [Fig. 3(k)].

Figure 4 shows the grain size distribution of semi-solid $Al_{80}Mg_5Li_5Zn_5Cu_5$ light-weight high-entropy alloy. When the isothermal temperature is 500 °C, the distribution range of the grain size increases from 30–55 μm at 15 min to 45–90 μm at 60 min, as shown in Fig. 4(a). When the isothermal temperature is 520 °C, as shown in Fig. 4(b), the distribution range of grain sizes increases from 20–45 μm at 15 min to 55–95 μm at 60 min. When the isothermal temperature increases to 540 °C, as shown in Fig. 4(c), the distribution range of grain sizes increases from 25–65 μm at 15 min to 65–100 μm at 60 min. The above data indicate that, with increasing the holding time, the grain size

distribution widens and the size inhomogeneity exacerbates.

Figure 5 shows the effects of different isothermal temperatures and holding times on the average grain size and shape factor of semi-solid microstructure. The average grain size reduces firstly and then increases with the prolonging of holding time, while it increases gradually at 540 °C with holding time, as shown in Fig. 5(a). When the isothermal temperature is 500 °C, the grain size turns to more refined after holding for 15 min than that of 5 min, at which time the size is 50.8 μm; after holding for 30 min, it does not alter much in size; prolonging the holding time to 60 min, its size increases to 70.5 μm. When the isothermal temperature is 520 °C, the grain size increases from 39.8 μm at 15 min to 82.1 μm at 60 min. When the isothermal temperature is 540 °C, the grain size increases from 39.3 μm at 5 min to 87.3 μm at 60 min. It can also be observed from Fig. 5(a) that the average grain size increases with increasing isothermal temperature when the holding time exceeds 30 min. This is mainly due to the merging growth and Ostwald ripening between adjacent grains. As shown in Fig. 5(b), the shape factor of all the samples increases firstly and then decreases with the prolonging of holding time, which means that the roundness of the grains gets better at first and then gets worse. The shape factor increases firstly due to the spheroidization of the merged grains, and then decreases owing to the abnormal growth of large grains resulting from Ostwald ripening [14]. The shape factor is up to 0.90 when the $Al_{80}Mg_5Li_5Zn_5Cu_5$ light-weight high-entropy alloy is treated at 520 °C for 30 min. Zhang et al. [17] pointed out that, when the shape factor $F > 0.8$, the semi-solid microstructure of the alloy is well globular and suitable for semi-solid forming.

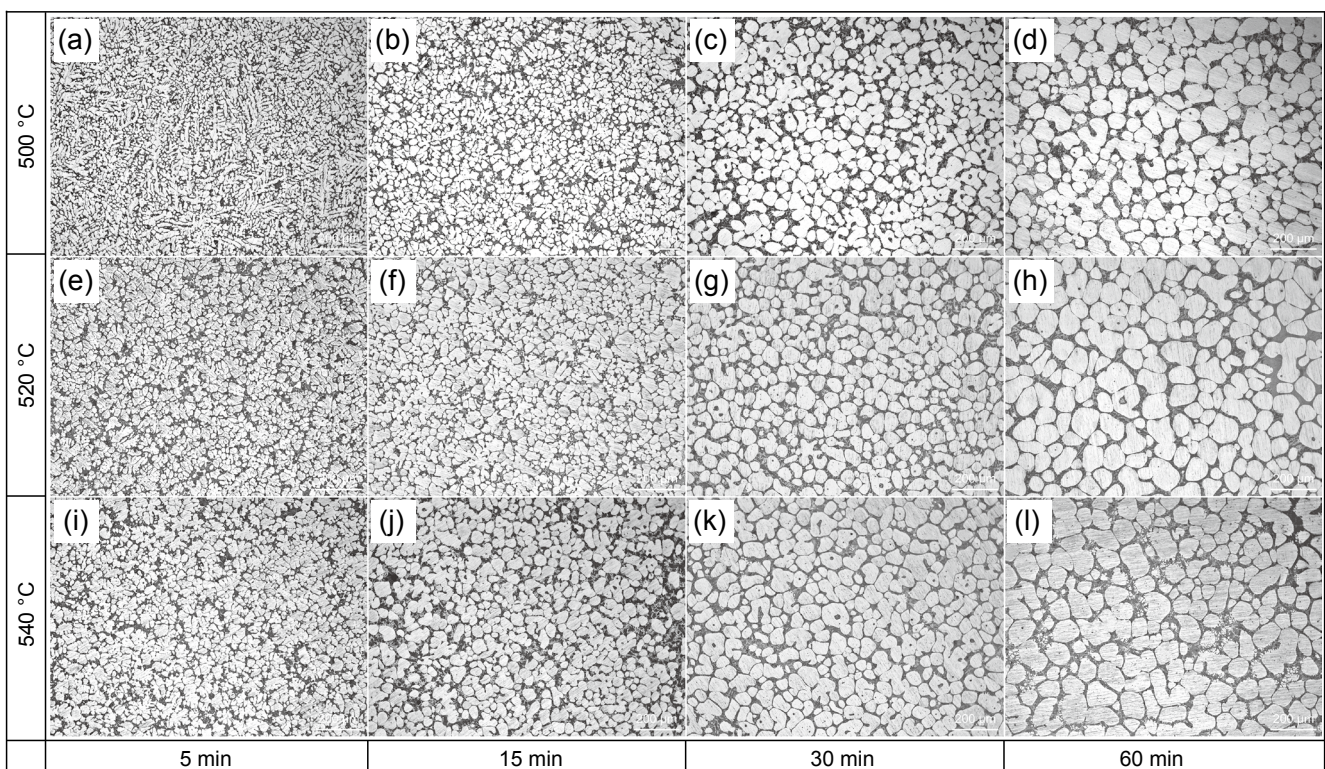


Fig. 3: Microstructures of $Al_{80}Mg_5Li_5Zn_5Cu_5$ light-weight high-entropy alloy treated at different temperatures for different times

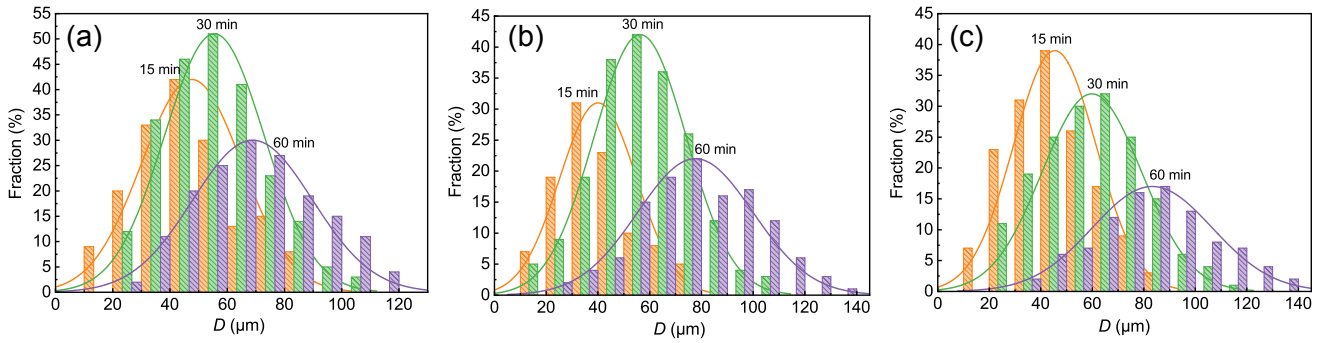


Fig. 4: Grain size distribution treated at 500 °C (a), 520 °C (b), and 540 °C (c) for different times

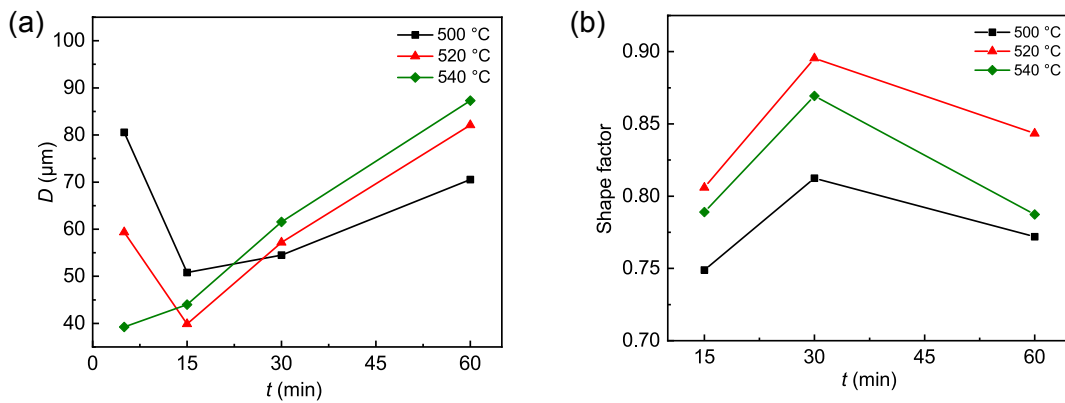


Fig. 5: Average grain size (a) and shape factor (b) of Al₈₀Mg₅Li₅Zn₅Cu₅ light-weight high entropy alloy

Figure 6 shows the SEM images of the as-cast and semi-solid (holding for 30 min at 520 °C) microstructures of Al₈₀Mg₅Li₅Zn₅Cu₅ light-weight high-entropy alloy, respectively. As shown in Fig. 6(b), the globular microstructure is α-Al phase of FCC structure. Comparing the segregation of Mg, Zn, and Cu elements at grain boundaries in as-cast microstructure [Fig. 6(a)], Mg and Zn elements distribute

uniformly in the whole alloy after holding for 30 min when the isothermal temperature is 520 °C, but Cu elements are mainly concentrated in the liquid phase. This is attributed to the different diffusion coefficients of Mg, Zn, and Cu elements in Al. The diffusion coefficient of Cu elements in Al is $4.8 \times 10^{-14} \text{ m}^2 \cdot \text{s}^{-1}$, which is much lower than that of Mg and Zn elements in Al of $1.2 \times 10^{-4} \text{ m}^2 \cdot \text{s}^{-1}$ and $4.9 \times 10^{-12} \text{ m}^2 \cdot \text{s}^{-1}$ [25, 26], respectively.

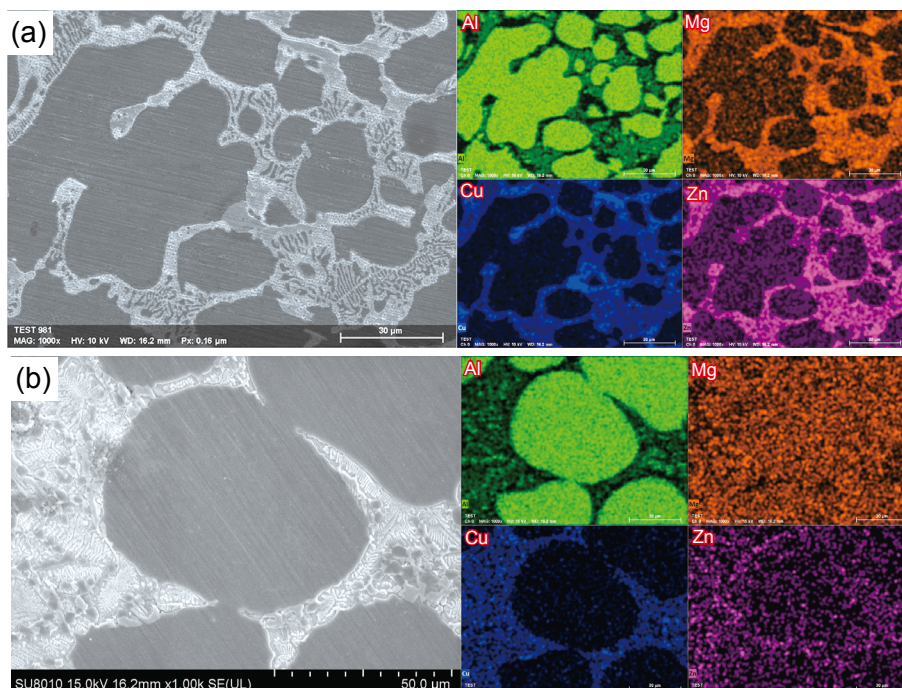


Fig. 6: SEM images and EDS maps of Al₈₀Mg₅Li₅Zn₅Cu₅ light-weight high-entropy alloy: (a) as-cast; (b) semi-solid after holding for 30 min at 520 °C

EBSDB results of $\text{Al}_{80}\text{Mg}_5\text{Li}_5\text{Zn}_5\text{Cu}_5$ light-weight high-entropy alloy are shown in Fig. 7 to further understand the microstructures. The phase identification results of $\text{Al}_{80}\text{Mg}_5\text{Li}_5\text{Zn}_5\text{Cu}_5$ light-weight high-entropy alloy are Al, Al_2Cu , Li_3CuAl_5 and MgZn_2 , which indicates that the phase constitutions remain basically unchanged after holding for 30 min at 520 °C, as shown in Fig. 7(b) and Fig. 7(e). The fractions of Al_2Cu and Li_3CuAl_5 in semi-solid microstructure are 10% and 15.5%, respectively, which are significantly

higher than those in as-cast microstructure. In semi-solid, MgZn_2 phases are fewer and distributed uniformly in the grain boundaries where Al_2Cu and Li_3CuAl_5 phases are mainly distributed, which is also consistent with the appearance of Cu-rich phase in Fig. 6(b). Combining with the inverse pole figure [Fig. 7(d)], Al_2Cu phases have a similar orientation to the Li_3CuAl_5 phases, while the grain orientations of MgZn_2 phases are relatively random in semi-solid microstructure.

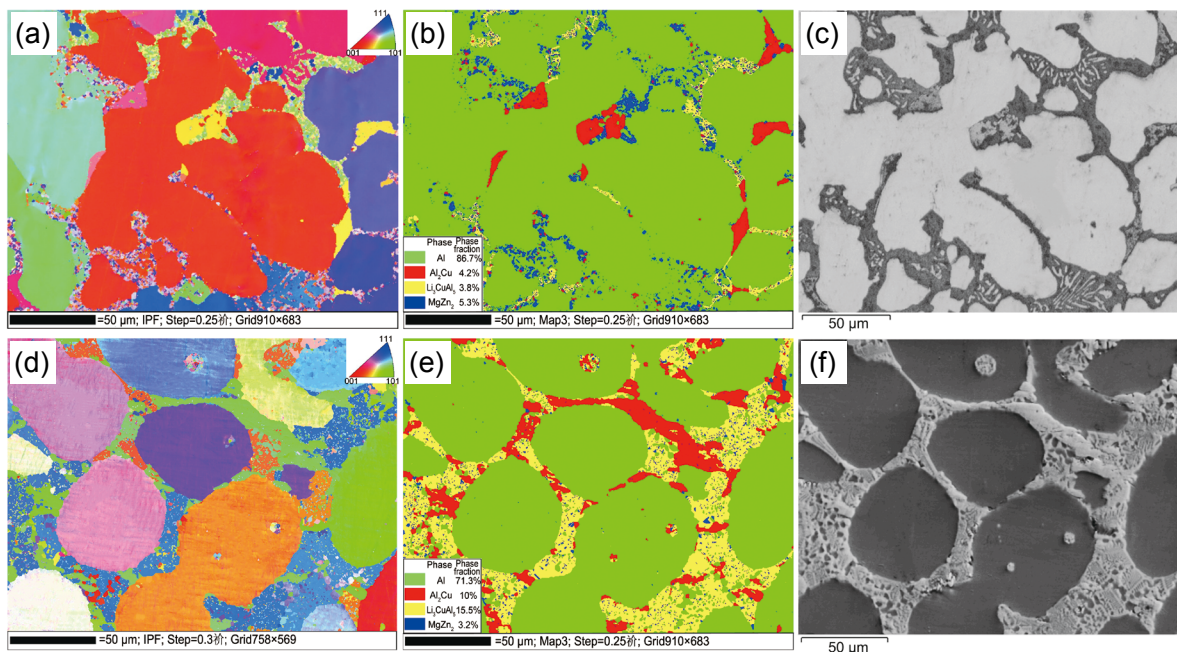


Fig. 7: EBSD analysis of as-cast (a-c) and semi-solid (d-f) $\text{Al}_{80}\text{Mg}_5\text{Li}_5\text{Zn}_5\text{Cu}_5$ light-weight high-entropy alloy

3.4 Compression property

Figure 8 shows the compressive properties of $\text{Al}_{80}\text{Mg}_5\text{Li}_5\text{Zn}_5\text{Cu}_5$ light-weight high-entropy alloy at room temperature. It can be found that, compared with the as-cast $\text{Al}_{80}\text{Mg}_5\text{Li}_5\text{Zn}_5\text{Cu}_5$ light-weight high-entropy alloy, the compressive strength of semi-solid $\text{Al}_{80}\text{Mg}_5\text{Li}_5\text{Zn}_5\text{Cu}_5$ light-weight high-entropy alloy treated at 520 °C for 30 min increases from 496.7 MPa to 676.5 MPa and the compressive plasticity increases from 9.5% to 19.8%, which are improved by 36% and 108%, respectively. The results reveal that the semi-solid $\text{Al}_{80}\text{Mg}_5\text{Li}_5\text{Zn}_5\text{Cu}_5$ light-weight high-entropy alloy after isothermal heat treatment exhibits high compressive strength (exceeding 550 MPa). It is well known that the mechanical properties of alloys are governed by the microstructures. Better compressive strength of semi-solid $\text{Al}_{80}\text{Mg}_5\text{Li}_5\text{Zn}_5\text{Cu}_5$ light-weight high-entropy alloy inherits from its fine microstructure. Meanwhile, the globular microstructures will rotate to coordinate deformation during compression, reducing stress concentration and increasing compressive strength. The compressive plasticity has a strong dependence on the morphology of microstructures^[27]. The shape factor of semi-solid $\text{Al}_{80}\text{Mg}_5\text{Li}_5\text{Zn}_5\text{Cu}_5$ light-weight high-entropy alloy is obviously higher than that of as-cast alloy, especially after isothermal heat treatment. The high degree of spheroidization of microstructures is helpful for

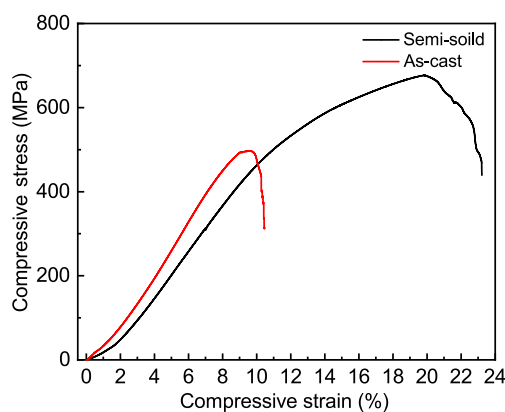


Fig. 8: Compressive engineering stress-strain curves of $\text{Al}_{80}\text{Mg}_5\text{Li}_5\text{Zn}_5\text{Cu}_5$ light-weight high-entropy alloy

obtaining good plasticity^[27]. Moreover, the segregation of Mg and Zn is reduced after isothermal heat treatment, as shown in Fig. 6, which can also improve the mechanical properties.

4 Discussion

The semi-solid microstructure of $\text{Al}_{80}\text{Mg}_5\text{Li}_5\text{Zn}_5\text{Cu}_5$ light-weight high-entropy alloy was successfully obtained in the present work. It is observed from Fig. 3 that the formation

of semi-solid microstructure includes three stages: melting separation, spheroidization, and coarsening growth.

In the initial stage of isothermal heat treatment, the grain boundaries with lower melting points melted firstly to irregular shape. Meanwhile, the curvatures (or curvature radius) at different positions for the dendrite arms are different. According to Gibbs-Thomson equation, the solute atomic concentration in the interface is related to the curvature radius^[28]:

$$C_{\alpha}(r) = C_{\alpha}(\infty)\exp(2\sigma V_B / K_B Tr) \quad (5)$$

where $C_{\alpha}(r)$ is the solute atomic concentration at the position with a curvature radius r ; $C_{\alpha}(\infty)$ is the solute atomic concentration at the flat interface; σ is the surface tension; V_B is the solute atomic volume; K_B is the shape factor; and T is the temperature.

According to Eq. (5), the smaller the curvature radius, the higher the solute atomic concentration. Since the curvature of the root of the dendrite arms is greater than that of the other positions, there is a gradient of atom concentration at different positions^[28]. Therefore, the solute atoms will continuously diffuse from the root of the dendrite arms to the other positions during the isothermal heat treatment process, breaking the previous atomic concentration balance. In order to maintain the atomic concentration balance, the root of the dendrite arms will dissolve to make the curvature radius become larger^[29], as shown in Fig. 3(a) and Fig. 3(b). This process is the melting separation process.

The surface of the freshly melted and separated microstructure is convex and uneven, as shown in Fig. 3(b), and some of the grains are not completely separated from each other but are in a partial adhesion. It is well known that the curvature of solid particles can obviously influence its melting point. According to the solidification thermodynamics, the equilibrium melting point of the alloy is related to the curvature of the grain surface^[30]:

$$\Delta T_r = -2\sigma T_m \omega k / \Delta H_m \quad (6)$$

where ΔT_r is the reduced value of equilibrium melting point; T_m is the solid-liquid interface melting point; σ is the solid-liquid interface tension; ΔH_m is the molar enthalpy change during the solid-liquid transition; ω is the solid phase molar volume; k is the solid-liquid interface curvature.

According to Eq. (6), it can be seen that there is an inverse relationship between the equilibrium melting point and curvature, that is, the higher the curvature, the lower the equilibrium melting point. The bulge, irregularities and edges of the grains will lead to a decrease of melting point. Therefore, the bulge, irregularities and edges of the grains will melt at first, resulting in the irregular grains to become globular or near globular, which is known as the spheroidization process, as shown in Fig. 3(f) and Fig. 3(g). The spheroidization process is also the key to the formation of semi-solid microstructures.

With the prolonging of holding time, coarsening growth, which is determined by the mechanism of mergence growth and Ostwald ripening, can be observed. Mergence growth

occurs by diffusion between adjacent grains in the same orientation^[31]. The adjacent grains with small grain orientation difference are in contact with each other under the action of liquid-solid interfacial tension. When $\gamma_{ss} < 2\gamma_{sl}$ is satisfied^[32] (γ_{ss} is the solid-solid interfacial energy and γ_{sl} is the solid-liquid interfacial energy), the adjacent grains merge into one through grain boundary migration to reduce the interface area and the system free energy.

At the later stage of isothermal heat treatment, the grains larger than the average size continue to coarsen under the driving force of interfacial energy and interfacial curvature, while the small grains gradually melt until they disappear, which is consistent with the Ostwald ripening mechanism. As shown in Fig. 3(l), some grains grow abnormally with a size of 130 μm when holding for 60 min at 540 $^{\circ}\text{C}$, and the morphology of the grains becomes worse with a shape factor of 0.8. Generally speaking, there is no liquid phase in the conventional recrystallization grain growth process. However, the coarsening growth of semi-solid microstructure is a coarsening process with the coexistence of solid-liquid phase, which is the boundary migration caused by the diffusion with solid-liquid phase contact. Lifshiz, Slyozov and Wanger^[33] proposed the classical theory of grain coarsening (LSW theory) when sufficient liquid phase occurred, which is applicable to the solid-liquid phase mixing systems. According to LSW theory^[33], the coarsening behavior of the grains can be expressed by:

$$D^3 - D_0^3 = kt \quad (7)$$

where D is the average size of the grains at time t , D_0 is the average size of the initial grains, k is the grain coarsening rate constant.

The relationship between D^3 and holding time t for the semi-solid $\text{Al}_{80}\text{Mg}_5\text{Li}_5\text{Zn}_5\text{Cu}_5$ light-weight high-entropy alloy at different temperatures is shown in Fig. 9. It can be seen from Fig. 9 that there is a linear relationship between D^3 and holding time t at different temperatures. The regression coefficients R^2 are all greater than 0.9, which indicates there is a good linear relationship between D^3 and holding time t . The coarsening rate constant k increases with increasing the

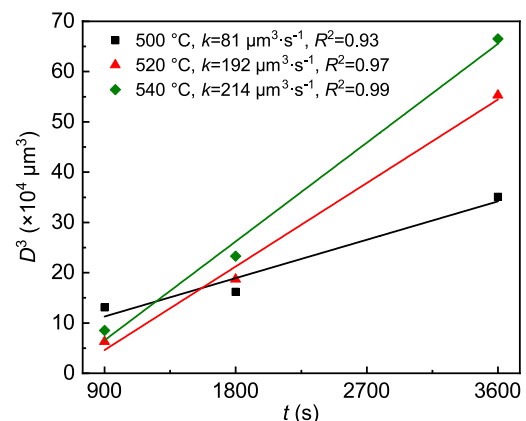


Fig. 9: Average grain size with holding time for $\text{Al}_{80}\text{Mg}_5\text{Li}_5\text{Zn}_5\text{Cu}_5$ light-weight high-entropy alloy at different isothermal temperatures

isothermal temperature, which means that the coarsening rate constant k increases with increasing the liquid phase volume fraction, which is consistent with the improved liquid film migration model. It is obvious that the coarsening rate constant increases from $81 \mu\text{m}^3\cdot\text{s}^{-1}$ to $214 \mu\text{m}^3\cdot\text{s}^{-1}$ when the temperature increases from $500 \text{ }^\circ\text{C}$ to $540 \text{ }^\circ\text{C}$. It indicates that the higher the temperature, the greater the effect of Ostwald ripening mechanism.

Figure 10 shows the coarsening rate constant for the conventional semi-solid alloys such as aluminum alloys and magnesium alloys. Compared with the conventional alloys, $\text{Al}_{80}\text{Mg}_5\text{Li}_5\text{Zn}_5\text{Cu}_5$ light-weight high-entropy alloy has a relatively low coarsening rate constant. It also can be found that CoCrCuFeNi high-entropy alloy also has a low coarsening rate constant. This is related to the sluggish diffusion effect of the high-entropy alloy. In the $\text{Al}_{80}\text{Mg}_5\text{Li}_5\text{Zn}_5\text{Cu}_5$ light-weight high-entropy alloy, the lack of a major diffusion element and the co-diffusion between the elements lead to the slow grain growth.

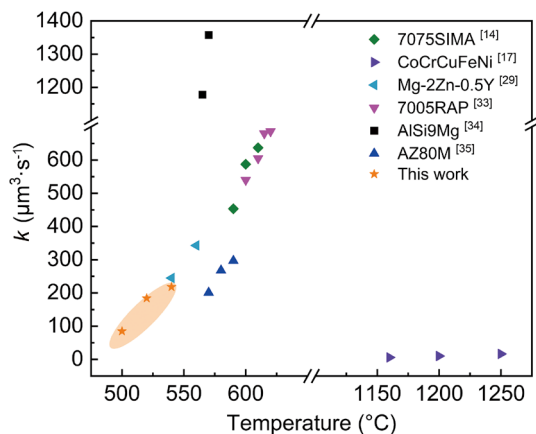


Fig. 10: Coarsening rate constant for $\text{Al}_{80}\text{Mg}_5\text{Li}_5\text{Zn}_5\text{Cu}_5$ of this study and for aluminum alloys, magnesium alloys, and CoCrCuFeNi of other studies

5 Conclusions

(1) Density of $\text{Al}_{80}\text{Mg}_5\text{Li}_5\text{Zn}_5\text{Cu}_5$ high-entropy alloy is $2.89 \text{ g}\cdot\text{cm}^{-3}$, less than $3 \text{ g}\cdot\text{cm}^{-3}$, belongs to light-weight high-entropy alloy.

(2) With isothermal temperature increasing, the average grain size of the $\text{Al}_{80}\text{Mg}_5\text{Li}_5\text{Zn}_5\text{Cu}_5$ alloy increases and the spheroidization time shortens. With the prolongation of holding time, the shape factor increases at first and then decreases. And the average grain size decreases firstly and then increases when the isothermal temperature is below $520 \text{ }^\circ\text{C}$, however it increases gradually at $540 \text{ }^\circ\text{C}$ with holding time. The optimal semi-solid microstructure is obtained at $520 \text{ }^\circ\text{C}$ for 30 min, whose shape factor and average grain size are 0.90 and $56.4 \mu\text{m}$, respectively. The $\text{Al}_{80}\text{Mg}_5\text{Li}_5\text{Zn}_5\text{Cu}_5$ light-weight high-entropy alloy has a low coarsening rate constant, which is attributed to the sluggish diffusion effect of the high-entropy alloy.

(3) The compressive strength and plasticity of the semi-solid

$\text{Al}_{80}\text{Mg}_5\text{Li}_5\text{Zn}_5\text{Cu}_5$ light-weight high-entropy alloy are 676.5 MPa and 19.8%, which are improved by 36% and 108%, respectively, compared with the as-cast $\text{Al}_{80}\text{Mg}_5\text{Li}_5\text{Zn}_5\text{Cu}_5$ light-weight high-entropy alloy.

(4) The formation of the semi-solid microstructure of $\text{Al}_{80}\text{Mg}_5\text{Li}_5\text{Zn}_5\text{Cu}_5$ light-weight high-entropy alloy includes three stages: melting separation, spheroidization and coarsening growth.

Acknowledgements

This work was financially supported by the National Natural Science Foundation of China (Grant No. 51865011) and the Natural Science Foundation of Jiangxi Province, China (Grant No. 20212BAB204008).

References

- [1] Guo N N, Wang L, Su Y Q, et al. Microstructure and properties of novel quinary multi-principal element alloys with refractory elements. *China Foundry*, 2015, 12(5): 319–326.
- [2] Kai W, Li C C, Cheng F P, et al. The oxidation behavior of an equimolar FeCoNiCrMn high-entropy alloy at $950 \text{ }^\circ\text{C}$ in various oxygen-containing atmospheres. *Corrosion Science*, 2016, 108: 209–214.
- [3] Cui Y, Shen J, Manladan S M, et al. Wear resistance of FeCoCrNiMnAl_x high-entropy alloy coatings at high temperature. *Applied Surface Science*, 2020, 512: 145736.
- [4] Qiu X W, Zhang Y P, He L, et al. Microstructure and corrosion resistance of AlCrFeCuCo high entropy alloy. *Journal of Alloys and Compounds*, 2013, 549: 195–199.
- [5] Cantor B, Chang I T H, Knight P, et al. Microstructural development in equiatomic multicomponent alloys. *Materials Science and Engineering: A*, 2004, 375: 213–218.
- [6] Cantor B. Multicomponent and high entropy alloys. *Entropy*, 2014, 16(9): 4749–4768.
- [7] Du X H, Wang R, Chen C, et al. Preparation of a light-weight MgCaAlLiCu high-entropy alloy. *Key Engineering Materials*, 2017, 727: 132–135.
- [8] Stepanov N D, Yurchenko N Y, Sokolovsky V S, et al. An $\text{AlNbTiVZr}_{0.5}$ high-entropy alloy combining high specific strength and good ductility. *Materials Letters*, 2015, 161: 136–139.
- [9] Xia M, Sun B, Wang X, et al. Research status and prospects of additive manufacturing of high entropy alloys. *Materials Reports*, 2021, 35(13): 13119–13127.
- [10] Joseph J, Hodgson P, Jarvis T, et al. Effect of hot isostatic pressing on the microstructure and mechanical properties of additive manufactured $\text{Al}_x\text{CoCrFeNi}$ high entropy alloys. *Materials Science and Engineering: A*, 2018, 733: 59–70.
- [11] Flemings M C. Behavior of metal alloys in the semisolid state. *Metallurgical Transactions A*, 1991, 22(5): 957–981.
- [12] Li D N, Luo J R, Wu S S, et al. Study on the semi-solid rheocasting of magnesium alloy by mechanical stirring. *Journal of Materials Processing Technology*, 2002, 129(1–3): 431–434.
- [13] Mohammed M N, Omar M Z, Salleh M S, et al. Semisolid metal processing techniques for nondendritic feedstock production. *The Scientific World Journal*, 2013, 2013: 752175.
- [14] Bolouri A, Shahmiri M, Cheshmeh E N H. Microstructural evolution during semisolid state strain induced melt activation process of aluminum 7075 alloy. *Transactions of Nonferrous Metals Society of China*, 2010, 20(9): 1663–1671.

- [15] Tao J Q, Wan Y Y, Sun C J, et al. Microstructure evolution of an Mg-Zn-Nd-Zr magnesium alloy during recrystallization and partial remelting process. *China Foundry*, 2013, 10(4): 244–247.
- [16] Yang M B, Pan F S, Cheng R J, et al. Effects of holding temperature and time on semi-solid isothermal heat-treated microstructure of ZA84 magnesium alloy. *Transactions of Nonferrous Metals Society of China*, 2008, 18(3): 566–572.
- [17] Zhang L J, Fan J T, Liu D J, et al. The microstructural evolution and hardness of the equiatomic CoCrCuFeNi high-entropy alloy in the semi-solid state. *Journal of Alloys and Compounds*, 2018, 745: 75–83.
- [18] Wang L J, Xiong J, Liu J, et al. Effect of microstructures and mechanical properties of large deformation high entropy alloy CoCrCuFeNi in semi-solid isothermal heat treatment. *Mechanical Engineering Science*, 2019, 1(2): 33–39.
- [19] Kim W T, Zhang D L, Cantor B. Nucleation of solidification in liquid droplets. *Metallurgical Transactions A*, 1991, 22(10): 2487–2501.
- [20] Jiang J F, Wang Y, Xiao G F, et al. Comparison of microstructural evolution of 7075 aluminum alloy fabricated by SIMA and RAP. *Journal of Materials Processing Technology*, 2016, 238: 361–372.
- [21] Aghaie-Khafri M, Azimi-Yancheshme D. The study of an Al-Fe-Si alloy after equal-channel angular pressing (ECAP) and subsequent semisolid heating. *JOM*, 2012, 64(5): 585–592.
- [22] Feng R, Gao M C, Lee C, et al. Design of light-weight high-entropy alloys. *Entropy*, 2016, 18(9): 333–353.
- [23] Gupta M, Tun K S. An insight into the development of light weight high entropy alloys. *Research & Development in Material Science*, 2017, 2: 9–11.
- [24] Shao L, Zhang T, Li L G, et al. A low-cost lightweight entropic alloy with high strength. *Journal of Materials Engineering and Performance*, 2018, 27(12): 6648–6656.
- [25] Neumann G, Tuijn C. Self-diffusion and impurity diffusion in pure metals: Handbook of experimental data. Elsevier, 2008.
- [26] Zhang W B. Investigation of diffusion coefficient and simulation of diffusion behavior in the multi-Al alloys. Changsha: Central South University, 2012.
- [27] Chen T, Xie Z W, Luo Z Z, et al. Microstructure evolution and tensile mechanical properties of thixoformed AZ61 magnesium alloy prepared by squeeze casting. *Transactions of Nonferrous Metals Society of China*, 2014, 24(11): 3421–3428.
- [28] Yang M B, Jia S, Pan F S. Effect of Sb on microstructure of semi-solid isothermal heat-treated AZ61-0.7Si magnesium alloy. *Transactions of Nonferrous Metals Society of China*, 2009, 19(1): 32–39.
- [29] Liu W, Yang D D, Quan G F, et al. Microstructure evolution of semisolid Mg-2Zn-0.5Y alloy during isothermal heat treatment. *Rare Metal Materials and Engineering*, 2016, 45(8): 1967–1972.
- [30] Feng K, Huang X F, Ma Y, et al. Microstructure evolution of ZA72 magnesium alloy during partial remelting. *China Foundry*, 2013, 10(2): 74–80.
- [31] Zhang C Y, Zhao S D, Wang Y F, et al. Microstructure evolution of semi-solid 2A50 alloy prepared by electromagnetic stirring method. *The Chinese Journal of Nonferrous Metals*, 2015, 25(7): 1781–1789.
- [32] Loue W R, Suery M. Microstructural evolution during partial remelting of Al₂Si₇Mg alloys. *Materials Science and Engineering A*, 1995, 203(1–2): 1–13.
- [33] Jiang J, Wang Y, Atkinson H V. Microstructural coarsening of 7005 aluminum alloy semisolid billets with high solid fraction. *Materials Characterization*, 2014, 90: 52–61.
- [34] Wang Y F, Guo Y, Zhao S D. Effects of process parameters on the microstructure and hardness of semi-solid AlSi9Mg aluminum alloy prepared by RAP process. *Materials Transactions*, 2020, 61(9): 1731–1739.
- [35] Fan L L, Zhou M Y, Zhang Y W X, et al. The semi-solid microstructural evolution and coarsening kinetics of AZ80-0.2Y-0.15Ca magnesium alloy. *Materials Characterization*, 2019, 154: 116–126.